TECHNICAL MEMORANDUM

657

The hydrostatic and nonhydrostatic global model IFS/ARPEGE: deep-layer model formulation and testing.

Karim Yessad[1] and Nils P. Wedi

Research Department

[1]Centre National de Recherches Météorologiques, Météo-France, Toulouse, France

December 2011

European Centre for Medium-Range Weather Forecasts
Europäisches Zentrum für mittelfristige Wettervorhersage
Centre européen pour les prévisions météorologiques à moyen terme

Series: ECMWF Technical Memoranda

A full list of ECMWF Publications can be found on our web site under:
http://www.ecmwf.int/publications/

Contact: library@ecmwf.int

European Centre for Medium-Range Weather Forecasts
Shinfield Park, Reading, RG2 9AX, England

Abstract

A nonhydrostatic dynamical core, formerly coded in the limited area model ALADIN, has been extended to the global model IFS/ARPEGE, for both the uniform and the rotated/stretched meshes, respectively. Options have been developed to run the global model under the spherical geopotential approximation using either the hydrostatic primitive equations, the quasi-hydrostatic equations, the nonhydrostatic shallow-atmosphere equations or the nonhydrostatic deep-atmosphere equations. The latter includes the additional accelerations in the zonal and vertical components of the momentum equation due to the Coriolis force and (optionally) the vertical variations of the gravitational acceleration. The nonhydrostatic deep model is equally stable compared with the hydrostatic shallow-atmosphere model when the aspect ratio of the vertical extent of the atmosphere compared to the radius of the sphere is $\ll 1$. The four different formulations are compared in idealised simulations as well as against results from the (optionally) shallow or deep nonhydrostatic EULAG model. Both the deep- and shallow-atmosphere IFS model versions give practically equivalent results in four-member ensembles of 13 months simulations, and practically equivalent statistics in medium-range weather forecasts, suggesting a negligible effect when the resolved flow regime is hydrostatic.

1 Introduction

The operational dynamical core of ECMWF's Integrated Forecasting System (IFS) and ARPEGE, its global equivalent at Meteo-France, is based on the hydrostatic primitive equations and is likely to be of limited use at horizontal scales finer than about 10 km, where nonhydrostatic effects will become important (ECMWF, 2000). Rather than developing such a dynamical core from scratch or investigate other existing formulations it was decided to evaluate the nonhydrostatic formulation (Bubnová et al., 1995) developed by the ALADIN group (ALADIN, 1997) and made available by Météo-France in the global IFS/ARPEGE model (Bénard et al., 2010; Yessad, 2011). The advantages of this nonhydrostatic dynamical core are the algorithmic proximity to the existing hydrostatic model framework and the underlying hydrostatic balance due to its formulation in terms of a deviation from this balance. A comprehensive summary of various tests performed during this assessment are discussed in Wedi et al. (2009), showing equivalent results and stability in the asymptotic limit of hydrostatic scales between the hydrostatic and the nonhydrostatic model formulation.

The prognostic equations of the IFS/ARPEGE dynamical core were derived under the philosophy of gradually extending the hydrostatic primitive equations to the fully compressible Euler equations (Ritchie et al., 1995; Laprise, 1992; Bubnová et al., 1995; Temperton et al., 2001; Bénard et al., 2005, 2010; Wedi et al., 2009) on the sphere. The assumption of sphericity of the Earth's surface and its influence on weather and climate simulations is not known, but theoretical developments suggest that "geophysical fluid dynamics can safely use a spherical coordinate system that can in first approximation be considered to be anchored on spherical iso-surfaces of the geopotential;..." (v. d. Toorn and Zimmerman, 2008). However, so far the IFS/ARPEGE model also neglects part of the zonal and vertical accelerations due to the Coriolis force and some metric terms related to the advection in the curvilinear spherical system, i.e. the so called shallow-atmosphere or "traditional" approximation is made. The hydrostatic system of equations — albeit its approximations — preserves the conservation principles for angular momentum, energy and potential vorticity (White and Bromley, 1995; White et al., 2005). Based on scale analysis White and Bromley (1995) suggested a potential influence of up to 10 percent variation in the average vertical or zonal acceleration in the tropics if the shallow-atmosphere approximation was relaxed. Gerkema et al. (2008) reviewed the influence of the additional Coriolis acclerations for different flow simulations. The authors show implications for interactions of waves and boundary layers and for regime transitions and wave interactions that may be relevant to large-scale atmospheric flow. Moreover,

Gerkema et al. (2008) stress that the biggest impact may be expected in weakly stratified flow in low latitudes. However, due to the limited vertical resolution of tropical boundary layers and the columnar physical parametrizations typically used in global models it is unclear if such effects could be seen in global atmospheric simulations, particularly when only resolving hydrostatic scales.

White et al. (2005) reviewed the four possible (energetically consistent) alternative equation sets on the sphere (i.e. the spherical geopotential approximation is made), cf. table 1 in White et al. (2005): the hydrostatic primitive equations (HPE), the nonhydrostatic shallow-atmosphere equations (NHS), the quasi-hydrostatic equations (QHE), and the nonhydrostatic deep equations (NHD). This paper extends their work by illustrating the differences obtained in the context of idealised flows (mainly to check the correctness of implementation), and by quantifying the differences in the context of numerical weather prediction (NWP) and climate simulations. The purpose of our paper is two-fold, to document the implementation of these four different equation sets in the IFS/ARPEGE system and to quantify their respective impact on NWP.

The HPE set represents the current operational setup of ECMWF's forecast model (Temperton et al., 2001). The NHS model has been described in the limited-area context in Bénard et al. (2010). Here the system of equations has been adapted to the sphere and represents the system of equations that has been used in various intercomparison studies, cf. Wedi and Smolarkiewicz (2009) and Wedi et al. (2009). The QHE set has been implemented following closely White and Bromley (1995). The NHD model has been implemented following the modelling framework proposed in Wood and Staniforth (2003). The QHE and NHD model represent two alternative approaches for including deep-layer effects, since a quasi-hydrostatic system may also be obtained by simplifying the NHD system. However, the QHE system had been implemented into the IFS structure several years before the emergence of a stable non-hydrostatic IFS/Arpege model and a quasi-hydrostatic variant starting from the NHD model does not currently exist in IFS.

Section 2 summarises the four equation sets and the modifications necessary in IFS/ARPEGE to convert the HPE system into either the QHE, NHS, or NHD model, respectively. Section 3 presents results for the different model formulations. Finally, section 4 discusses some practical advantages and disadvantages of the NHS and NHD formulations and concludes the paper.

2 Model formulation

This section briefly summarises the HPE formulation of the IFS/ARPEGE model while focusing on the relevant differences to the HPE model for each of the extended model formulations, namely QHE, NHS, and the NHD model. For convenience all symbols and definitions are explained in table 2.

2.1 General

The total derivative operator $d/dt \equiv \partial/\partial t + \mathbf{V}\cdot\nabla + \dot{\eta}\partial/\partial\eta$, is discretised in a two-time-level semi-Lagrangian fashion, for details of the discretisation and the model formulation see Ritchie et al. (1995); Temperton et al. (2001). The semi-implicit time discretisation — initially proposed by Robert et al. (1972) for the hydrostatic equations — is derived by subtracting from the governing model equations a system of equations linearised around an isothermal, quiescent, hydrostatically balanced and horizontally homogeneous reference state. The linear part is treated implicitly, whereas the discretisation of the nonlinear residual is explicit (Bénard, 2003, 2004; Bénard et al., 2004, 2005). The resulting linear system

of equations can be reduced by suitable elimination of variables to a single Helmholtz equation which is solved in spectral space. The linear Coriolis terms in both the hydrostatic as well as the nonhydrostatic IFS may be treated either as part of the advected prognostic variables or implicitly together with the linear terms arising from the semi-implicit model (Temperton, 1997) (although such a formulation can be implemented only in the unstretched unrotated version of IFS/ARPEGE). For the QHE, NHS and NHD model the implicit treatment of the Coriolis force had to be suitably modified to fit the revised semi-implicit elimination process of the nonhydrostatic model (Yessad, 2011). All tests shown in this paper have used the implicit treatment of the Coriolis terms.

The evolution equations of the IFS/ARPEGE are cast in a terrain following mass-based coordinate (Simmons and Burridge, 1981; Laprise, 1992)

$$\Pi = A + B\Pi_s \tag{1}$$

where $(A(\eta), B(\eta))$ represent a pre-defined set of constants and η denotes the hybrid vertical coordinate. The vertical discretisation is optionally finite-difference (Ritchie et al., 1995) or finite-element (Untch and Hortal, 2004), the latter being used in the operational IFS model at ECMWF. To facilitate comparison of the four different model formulations and to minimise differences, the finite-difference discretisation in the vertical has been used for all results presented in this paper unless stated otherwise. Moreover, the iterative-centered-implicit (ICI) algorithm has been applied in all simulations with one iteration, see Bénard et al. (2010) and also Wedi et al. (2009) for a discussion.

Notably, a two-dimensional horizontal rotation operator (Temperton et al., 2001; Staniforth et al., 2010; Wood et al., 2010) is used to "transport" vectors along the semi-Lagrangian trajectory. Trajectories are great circles on the geographical sphere. The computation of the location of the medium point of the trajectory is performed by an iterative procedure (Robert, 1981) and adapted to the sphere by M. Rochas (internal note, Meteo-France). This has the consequence that some curvature terms are hidden in the Lagrangian form of the equations, in particular the terms $UV\tan\theta/r$ and $-U^2\tan\theta/r$. This operator is unchanged in the deep-layer formulations but there are additional terms to be considered in the QHE and NHD models, namely the previously neglected contributions due to the Coriolis force in the right-hand-sides of the zonal momentum equation, $2\Omega W\cos\theta$, the additional vertical acceleration $2\Omega U\cos\theta$, and the additional metric terms $-W\mathbf{V}/r$ and $(U^2+V^2)/r$. A recent discussion on this approach may be found in Thuburn and White (2012), who suggest that a splitting of horizontal and vertical motions before discretisation facilitates the application of the same "shallow-atmosphere" rotation matrix (Staniforth et al., 2010). This is particularly useful when the prognostic variable describing the vertical motion is not the vertical velocity w. The additional terms are treated numerically like the pressure gradient term and this appears to be stable. In addition, the velocity used to find the medium/departure point of the semi-Lagrangian trajectory in the NHD model is then $(a/r)\mathbf{V}$, instead of $\mathbf{V}$ in the HPE case.

2.2 HPE, without deep-layer effects

The governing equations and auxiliary relations of the hydrostatic system may be summarised as follows:

∗ **Momentum equation**

$$\frac{d\mathbf{V}}{dt} = -2(\Omega\times\mathbf{V}) - \nabla\Phi - RT\nabla(\log\Pi) + \mathbf{P}_\mathbf{V} \tag{2}$$

∗ **Thermodynamic equation**

$$\frac{dT}{dt} = \frac{RT}{c_{\mathrm{p}}}\frac{\omega}{\Pi} + P_{\mathrm{T}} \tag{3}$$

∗ **Vertically integrated Lagrangian formulation of the continuity equation**

$$\begin{aligned}&\int_0^1 \frac{\partial B}{\partial \eta}\frac{d\log\Pi_{\mathrm{s}}}{dt}d\eta = \\ &\int_0^1 \frac{\partial B}{\partial \eta}\left[-\frac{1}{\Pi_{\mathrm{s}}}\int_0^1 \nabla\cdot(m\mathbf{V})\,d\eta + \mathbf{V}\cdot\nabla\left(\log\Pi_{\mathrm{s}}\right)\right]d\eta,\end{aligned} \tag{4}$$

where the boundary conditions $[m\dot{\eta}]_{\eta=1} = 0$ and $[m\dot{\eta}]_{\eta=0} = 0$ have been used.

∗ **Vertical velocities ω and $m\dot{\eta}$**

$$[m\dot{\eta}]_{\eta_l} = B_{\eta_l}\int_0^1 \nabla\cdot(m\mathbf{V})\,d\eta - \int_0^{\eta_l}\nabla\cdot(m\mathbf{V})\,d\eta \tag{5}$$

and

$$\left[\frac{\omega}{\Pi}\right]_{\eta_l} = \left[\frac{1}{\Pi}\frac{d\Pi}{dt}\right]_{\eta_l} = \left[\mathbf{V}\cdot\frac{\nabla\Pi}{\Pi}\right]_{\eta_l} - \frac{1}{\Pi_{\eta_l}}\int_0^{\eta_l}\nabla\cdot(m\mathbf{V})\,d\eta \tag{6}$$

∗ **Tracer equations (e.g. specific humidity, cloud liquid water, cloud ice, rain, snow, etc.)**

$$\frac{dq_i}{dt} = P_{\mathrm{q}_i} \tag{7}$$

∗ **Relationship between geopotential height and pressure depth**

$$\frac{\partial\Phi}{\partial\Pi} = -\frac{RT}{\Pi}, \tag{8}$$

where $\Phi = g_0 z$.

2.3 QHE, with deep-layer effects

Following White and Bromley (1995) some modifications are required to consistently include deep-layer effects into the hydrostatic model. In this case the structure of the equations closely follows the HPE equations, but the approximations introduced to the equations are more than would be required, especially when comparing to Wood and Staniforth (2003). The distance to the Earth's centre is now the vertically-varying pseudo-radius r_π instead of the previously constant a. The essence of the approximation in the QHE model is the assumption that the radius depends only on the hydrostatic pressure. Thus two neighbouring vertical lines are no longer parallel, and the sectional volume slice of a vertical column varies with altitude.

The expression for radius r_π writes

$$r_\pi(\Pi) = a + \int_{\Pi}^{\Pi_{S,r}} \frac{R_\mathrm{d} T_\mathrm{r}(\Pi')}{g_0 \Pi'} d\Pi', \tag{9}$$

where a pre-defined reference temperature profile $T_\mathrm{r}(\Pi)$ that depends on the hydrostatic pressure has been used.

The diagnosed vertical velocity

$$W \equiv \frac{dr_\pi}{dt} = -\frac{R_\mathrm{d} T_\mathrm{r} \omega}{g_0 \Pi} \tag{10}$$

is now taken into account in the additional Coriolis accelerations and additional curvature terms. The gravitational acceleration is vertically constant.

The governing equations and auxiliary relations may then be summarised as follows:

∗ **Momentum equation**

$$\begin{aligned} \frac{d\mathbf{V}}{dt} = &- 2\Omega \times \mathbf{V} - 2\Omega \times W\mathbf{k} - \frac{W}{r_\pi}\mathbf{V} \\ &- \nabla\Phi - (RT + \mu_\mathrm{s} R_\mathrm{d} T_\mathrm{r})\nabla(\log\Pi) + \mathbf{P}_\mathbf{V}, \end{aligned} \tag{11}$$

where μ_s is defined as

$$\mu_\mathrm{s} \equiv -\frac{2\Omega r_\pi U \cos\theta + U^2 + V^2}{r_\pi g_0}. \tag{12}$$

The horizontal gradient operator ∇ is calculated in spectral space using a in the denominator. Thus for deep-layer models, the gradients resulting from the inverse transform (spectral to grid-point) are multiplied with r_π/a in the QHE and r/a in the NHD model, respectively.

∗ **Vertically integrated Lagrangian formulation of the continuity equation**

$$\begin{aligned} &\int_0^1 \frac{\partial B}{\partial \eta} \frac{d\log\Pi_\mathrm{s}}{dt} d\eta = \\ &\int_0^1 \frac{\partial B}{\partial \eta} \left[-\left(\frac{a^2}{{r_\pi}^2}\right)_{\eta=1} \frac{1}{\Pi_\mathrm{s}} \int_0^1 \left[\frac{r_\pi}{a}\nabla\right] \cdot \left(\frac{r_\pi}{a} m\mathbf{V}\right) d\eta \right] d\eta \\ &+ \int_0^1 \frac{\partial B}{\partial \eta} \left[\frac{a}{r_\pi}\mathbf{V} \cdot \left[\frac{r_\pi}{a}\nabla\right] (\log\Pi_\mathrm{s}) \right] d\eta \end{aligned} \tag{13}$$

∗ **Vertical velocities ω and $m\dot{\eta}$**

$$\begin{aligned} [m\dot{\eta}]_{\eta_l} = &B_{\eta_l} \left(\frac{a^2}{{r_\pi}^2}\right)_{\eta=1} \int_0^1 \left[\frac{r_\pi}{a}\nabla\right] \cdot \left(\frac{r_\pi}{a} m\mathbf{V}\right) d\eta \\ &- \left(\frac{a^2}{{r_\pi}^2}\right)_{\eta_l} \int_0^{\eta_l} \left[\frac{r_\pi}{a}\nabla\right] \cdot \left(\frac{r_\pi}{a} m\mathbf{V}\right) d\eta \end{aligned} \tag{14}$$

and

$$\left[\frac{r_\pi^2}{a^2}\frac{\omega}{\Pi}\right]_{\eta_l} = \left[\frac{1}{\Pi}\frac{r_\pi^2}{a^2}\frac{d\Pi}{dt}\right]_{\eta_l} = \left[\frac{r_\pi}{a}\mathbf{V}\cdot\frac{(r_\pi/a)\nabla\Pi}{\Pi}\right]_{\eta_l} - \frac{1}{\Pi_{\eta_l}}\int_0^{\eta_l}\left[\frac{r_\pi}{a}\nabla\right]\cdot\left(\frac{r_\pi}{a}m\mathbf{V}\right)d\eta \tag{15}$$

∗ **Relationship between geopotential height and pressure depth**

$$\frac{\partial\Phi}{\partial\Pi} = -\frac{RT}{\Pi}\left(1+\frac{R_\mathrm{d}T_\mathrm{r}}{RT}\mu_\mathrm{s}\right). \tag{16}$$

The thermodynamic and tracer equations are unchanged, cf. equations (3) and (7), respectively.

2.4 NHS, without deep-layer effects

In the NHS system there is a distinction between the hydrostatic pressure defined by the relationship $\partial\Pi/\partial z = -\rho g$ and the total pressure $p = \rho RT$. Compared to the HPE system, there are two additional prognostic variables to express the nonhydrostatic effects, a prognostic variable based on the pressure departure from hydrostatic pressure and a prognostic variable related to the vertical velocity or vertical divergence, see Bénard et al. (2010) and references therein. The vertical acceleration assumes the value $g = g_0$ in this case.

The governing equations of the NHS system and its auxiliary relations are summarised as follows:

∗ **Momentum equation**

$$\frac{d\mathbf{V}}{dt} = -2\Omega\times\mathbf{V} - \frac{\partial p}{\partial\Pi}\nabla\Phi - RT\frac{\nabla p}{p} + \mathbf{P}_\mathbf{V} \tag{17}$$

∗ **Thermodynamic equation**

$$\frac{dT}{dt} = -\frac{RT}{c_\mathrm{v}}D_3 + \frac{c_\mathrm{p}}{c_\mathrm{v}}P_\mathrm{T}, \tag{18}$$

where D_3 is computed as

$$D_3 = D + \mathscr{X} + \frac{R_\mathrm{d}}{R}d \tag{19}$$

and

$$\mathscr{X} = \frac{p}{mRT}\nabla\Phi\cdot\left(\frac{\partial\mathbf{V}}{\partial\eta}\right) \tag{20}$$

In the NHS system the continuity equation and vertical velocities ω and $m\dot{\eta}$ are unchanged, cf. equations (4), (5) and (6), respectively; the tracer equations are as determined in equation (7).

∗ **Pressure departure variable equation**

$$\frac{d\hat{Q}}{dt} = -\frac{c_\mathrm{p}}{c_\mathrm{v}}D_3 - \frac{\omega}{\Pi} + \frac{c_\mathrm{p}}{c_\mathrm{v}T}P_\mathrm{T}, \tag{21}$$

where $\hat{Q} \equiv \log(p/\Pi)$ is chosen to ensure that total pressure p always remains positive.

∗ **Vertical velocity w and vertical divergence d equations** There are two options for the choice of the advected vertical prognostic variable: either the vertical velocity w is advected (GWADV) or the alternative variable $d_4 \equiv d + \mathscr{X}$, where $d \equiv -(g_0 p/mR_dT)\partial w/\partial\eta$, cf. (Bénard et al., 2010). The former case is closer to the natural choice of prognostic vertical variable and the treatment of the lower boundary condition is simpler. However, d_4 is naturally defined on full levels and w is not, see also appendix B. Moreover, the GWADV option requires an explicit conversion from w to d_4, because the variable d_4 is used in the linear part of the semi-implicit scheme in the NHS/NHD model to ensure stability. The vertical velocity equation is given as

$$\frac{dw}{dt} = g_0 \frac{\partial(p-\Pi)}{\partial\Pi} + P_w \tag{22}$$

whereas the vertical divergence equation (see appendix A for the derivation) is

$$\begin{aligned}\frac{dd}{dt} = &- dD_3 + d\nabla\cdot\mathbf{V} - \frac{g_0 p}{mR_dT}\frac{\partial\left[dw/dt\right]_{ad}}{\partial\eta} \\ &+ \frac{g_0 p}{mR_dT}(\nabla w)\cdot\left(\frac{\partial\mathbf{V}}{\partial\eta}\right) + P_d\end{aligned} \tag{23}$$

with subscript $_{ad}$ denoting the adiabatic part only, while $P_d \equiv -(g_0 p/mR_dT)\partial P_w/\partial\eta$. At the surface the diagnostic relation

$$w_s = \mathbf{V}_s\cdot\nabla\Phi_s \tag{24}$$

is used.

∗ **Relationship between geopotential height and pressure depth**

$$\frac{\partial\Phi}{\partial\Pi} = -\frac{RT}{p}, \tag{25}$$

with $\Phi = g_0 z$.

If the GWADV option is not used, d_4 is the prognostic variable with a special semi-Lagrangian treatment near the lower boundary, cf. Wedi et al. (2009), Bénard et al. (2010) and references therein for details. All NHS and NHD simulations in this paper have used the GWADV option.

2.5 NHD, with deep-layer effects

Following Wood and Staniforth (2003) deep-layer effects are consistently included into the NHS system by means of a coordinate transformation. A mass-based vertically integrated quantity $\tilde{\Pi}$ is introduced to hide some explicit metric terms, especially in the continuity equation where $\tilde{\Pi}$ replaces Π. The latter may be obtained diagnostically when needed. The distance to the Earth's centre is now the vertically-varying radius r instead of the previously constant a in the HPE/NHS case and instead of the pseudo-radius r_π in the QHE case. Optionally the vertical variation of g may also be taken into account via $g \equiv Ga^2/r^2$. In addition, the prognostic vertical velocity $w \equiv dr/dt$ is now used in the additional Coriolis and curvature terms instead of the diagnosed quantity used in the QHE model.

∗ **Relationship between $\tilde{\Pi}$ and Π**

$$\frac{\partial\tilde{\Pi}}{\partial r} = -\rho G\frac{r^2}{a^2} \tag{26}$$

defines $\tilde{\Pi}$ and

$$\frac{\partial \Pi}{\partial r} = -\rho g \tag{27}$$

defines Π. Combining (26) and (27) yields

$$\frac{\partial \tilde{\Pi}}{\partial \Pi} = \frac{r^2}{a^2}\frac{G}{g}. \tag{28}$$

In IFS the simulated vertical depth of the atmosphere (taken as the top model level) is typically 80 km versus 6370 km Earth radius, resulting in the ratio $r^2/a^2 \approx 1.025$. If vertical variations of g are taken into account relation (28) becomes $r^4/a^4 \approx 1.05$. The model top is chosen as a reference level where $\tilde{\Pi} = \Pi$, which ensures that $\tilde{\Pi}$ always remains > 0. Note that Π must be retrieved from relationship (28) knowing $\tilde{\Pi}$ and r instead of relation (1), because now

$$\tilde{\Pi} = A + B\tilde{\Pi}_s. \tag{29}$$

For a real atmosphere or an idealised scenario where the depth of the atmosphere remains small compared to the radius of the planet, $\tilde{\Pi}$ remains close to Π. For example, $\tilde{\Pi}_s - \Pi_s$ is approximately 200 Pa for actual simulations of weather and climate. One consequence of this is, when a set of (A,B)s has been defined for the HPE or NHS model, the same set of (A,B)s can be kept in the NHD model without significantly altering the relative vertical staggering. However, for idealised cases, e.g. a small planet, this is no longer true. $\tilde{\Pi}_s - \Pi_s$ can reach the same order of magnitude as Π_s, and in this case one cannot directly re-use the pre-defined set of (A,B)s in the NHD simulations. In order to accommodate idealised simulations on small planets, a second set of (A,B)s is defined. Appendix C describes the conversion formulae, typical values and the required iterative procedure to retrieve $\tilde{\Pi}$ and r when only Π is known from the initial conditions.

The radius r is obtained from the definition of $\tilde{\Pi}$ (Wood and Staniforth, 2003):

$$\frac{G}{3a^2}r^3 = \frac{G}{3a^2}r_s^3 - \int_{\tilde{\Pi}'=\tilde{\Pi}_s}^{\tilde{\Pi}'=\tilde{\Pi}} \frac{RT}{p} d\tilde{\Pi}' \tag{30}$$

and $r_s = a + z_s$, where z_s is the height of the orography. Note that $\Phi_s \equiv G r_s$.

The governing equations of the NHD system and its auxiliary relations may now be summarised as follows:

∗ **Momentum equation**

$$\begin{aligned}\frac{d\mathbf{V}}{dt} =& -2\Omega \times \mathbf{V} - 2\Omega \times w\mathbf{k} - \frac{w}{r}\mathbf{V} \\ & - \frac{r^2}{a^2}\frac{\partial p}{\partial \tilde{\Pi}}\nabla(Gr) - RT\frac{\nabla p}{p} + \mathbf{P}_\mathbf{V},\end{aligned} \tag{31}$$

The thermodynamic equation is identical to equation (18) of the NHS model but the expression for D_3 (cf. equation (4.14) in Wood and Staniforth (2003)) writes

$$\begin{aligned}D_3 =& \nabla \cdot \mathbf{V} + \frac{r^2}{a^2}\frac{p}{\tilde{m}RT}\nabla[Gr] \cdot \left(\frac{\partial \mathbf{V}}{\partial \eta}\right) \\ & - \frac{Gp}{\tilde{m}RT}\left(\frac{\partial (r^2/a^2)w}{\partial \eta}\right)\end{aligned} \tag{32}$$

∗ **Vertically integrated Lagrangian formulation of the continuity equation**

$$\int_0^1 \frac{\partial B}{\partial \eta}\frac{d\log\tilde{\Pi}_s}{dt}d\eta = \int_0^1 \frac{\partial B}{\partial \eta}\left[-\frac{1}{\tilde{\Pi}_s}\int_0^1 \nabla\cdot\left(\frac{a}{r}\tilde{m}\mathbf{V}\right)d\eta + \mathbf{V}\cdot\nabla\left(\log\tilde{\Pi}_s\right)\right]d\eta, \tag{33}$$

where, compared to the continuity equation (4), Π has been changed into $\tilde{\Pi}$ and $\nabla\cdot(m\mathbf{V})$ into $\nabla\cdot\left(\frac{a}{r}\tilde{m}\mathbf{V}\right)$. Similarly, using $\tilde{\omega}\equiv d\tilde{\Pi}/dt$ and the previous replacements, equations (5) and (6) change correspondingly. The tracer equations are as determined in equation (7).

∗ **Pressure departure variable equation**

The prognostic variable of the NHS model $\hat{Q}\equiv\log(p/\Pi)$ is not suitable as the prognostic variable in the NHD model because only $\tilde{\omega}$ and not ω is available, cf. equation (21). The simplest alternative is to use $\log(p/\tilde{\Pi})$ but $\log(p/\tilde{\Pi}) = \log(p/\Pi)+\log(\Pi/\tilde{\Pi})$. However, for nearly hydrostatic flows $\log(\Pi/\tilde{\Pi})$ is significantly larger than $\log(p/\Pi)$. In addition, $\log(\Pi/\tilde{\Pi})$ remains close to a mean value but with a vertical gradient, which is likely to be less accurate in connection with the semi-Lagrangian advection scheme. For this reason the revised prognostic variable $\hat{Q}$ is chosen as

$$\hat{Q}\equiv\log\left(\frac{p}{\tilde{\Pi}}\right)+\delta_P\log\left(\frac{\tilde{\Pi}_r}{\Pi_r}\right), \tag{34}$$

where $\tilde{\Pi}_r$ and Π_r are reference values based on the standard atmosphere. Note that $\log(\tilde{\Pi}_r/\Pi_r)$ is time independent and constant along η-surfaces. It is desirable to take a value of δ_P close to 1; optimal values have been found as between 1 and 1.1. With this definition the pressure departure variable equation (cf. equation (21) and equation (4.8) in Wood and Staniforth (2003)) writes

$$\frac{d\hat{Q}}{dt} = -\frac{c_p}{c_v}D_3 - \frac{\tilde{\omega}}{\tilde{\Pi}} + \delta_P\dot{\eta}\frac{\partial\log(\tilde{\Pi}_r/\Pi_r)}{\partial\eta} + \frac{c_p}{c_v T}P_T \tag{35}$$

∗ **Vertical velocity** w **and vertical divergence** d **equations**

$$\frac{dw}{dt} = -G\mu_s - (g-G) - G\left(1-\frac{r^2}{a^2}\right)\frac{\partial p}{\partial\tilde{\Pi}} + G\frac{\partial(p-\tilde{\Pi})}{\partial\tilde{\Pi}} + P_w \tag{36}$$

Compared to the NHS model an additional metric term appears related to the vertical variation, $G\left(1-r^2/a^2\right)\partial p/\partial\tilde{\Pi}$, and an additional term containing μ_s, cf. equation (12), whose two parts are due to the Coriolis force and due to the advection in the curvilinear spherical system.

The vertical divergence d is defined in the NHD model as

$$d\equiv-\frac{Gp}{\tilde{m}R_d T}\left(\frac{\partial(r^2/a^2)w}{\partial\eta}\right), \tag{37}$$

where the factor r^2/a^2 reflects the fact that the size of horizontal sections is no longer vertically independent. The definition (and the IFS code) uses the gas constant for dry air R_d here rather than R but there appears to be no reason in principle why d could not be defined in terms of R instead. With this definition the vertical divergence equation (see appendix A for the derivation) is

$$\frac{dd}{dt} = -dD_3 + d\nabla\cdot\mathbf{V} - \frac{Gp}{\tilde{m}R_{\mathrm{d}}T}\frac{\partial[d[(r^2/a^2)w]/dt]_{\mathrm{ad}}}{\partial\eta} + \frac{Gp}{\tilde{m}R_{\mathrm{d}}T}\left(\nabla\left[\frac{r^2}{a^2}w\right]\right)\cdot\frac{\partial\mathbf{V}}{\partial\eta} + P_{\mathrm{d}} \tag{38}$$

where subscript $_{\mathrm{ad}}$ again denotes the adiabatic part only and $P_{\mathrm{d}} \equiv -(Gp/\tilde{m}R_{\mathrm{d}}T)\partial P_w/\partial\eta$. Equations (38) and (36) may be combined together using the relation

$$\frac{d\left[(r^2/a^2)w\right]}{dt} = \frac{r^2}{a^2}\frac{dw}{dt} + 2\frac{r}{a^2}w^2. \tag{39}$$

Notably, for the GWADV option only equation (36) and definition (37) are required to retrieve d from w or vice versa. We have developed switches in the NHD model to isolate the effects due to the Coriolis and advection terms in the spherical system from the effects due to the vertical variations of $r-a$ and g, respectively.

The linear system is unchanged compared to the NHS model. Experimentation shows that the same value of the reference pressure (Bénard, 2003) may be used, as long as $\tilde{\Pi}$ does not deviate substantially from Π.

For post-processing and the coupling to the physical parametrizations $\tilde{\Pi}$ is converted into Π, with the physical parametrizations unchanged compared to the NHS model.

It is necessary to specify initial conditions for vertical divergence d, $\mathscr{X}$ and the nonhydrostatic pressure departure $\hat{Q}$. Initial conditions derived from the ECMWF analysis are hydrostatic and the additional variables are computed specifying the nonhydrostatic pressure departure ($\equiv 0$) and diagnose vertical velocity. A preliminary conversion is necessary to retrieve r and $\tilde{\Pi}$ from Π,using the iterative algorithm described above, to derive $p-\tilde{\Pi}$ from $p-\Pi$, and finally to compute an initial $\hat{Q}$. The variable $\mathscr{X}$ is diagnosed from the initial values of $\mathbf{V}$, $\tilde{\Pi}$, RT, and Φ. The initial vertical divergence d is then computed, postulating that initially dT/dt is the same in the NHD and the HPE model, i.e. equating the right-hand-sides of (3) and (18).

3 Results

Results are presented for the four different model formulations introduced in the previous section, highlighting specific differences arising from the model formulations and their respective approximations. However, the vertical variation of g is neglected in all simulations in this section, i.e. $g \equiv g_0$. The small-planet simulations presented here have been included to test the correctness of the implementation and the stability of the numerical procedure. Additional idealised simulations have been done with the EULAG model (Prusa et al., 2008) as an independent reference. Finally, equivalent simulations with IFS HPE, QHE and NHD formulation, respectively, attempt to quantify the effect of relaxing the shallow-atmosphere approximation in the context of NWP and climate.

The Held-Suarez (Held and Suarez, 1994) simulations, introduced as a test-bed on reduced-size planets in Smolarkiewicz et al. (1999) and more recently in Wedi and Smolarkiewicz (2009), evaluate the

influence of the dynamical core formulation on an idealised 'climate' state on the sphere. The Held-Suarez setup consists of dynamical core simulations, where the effect of the physics is emulated by adding the frictional term $-k_{\mathbf{v}}\mathbf{v}$ on the rhs of the momentum equation and adding $-k_T(T-T_{eq})$ in the thermodynamic equation, where $k_{\mathbf{v}}, k_T$ denote frictional/heating coefficients and T_{eq} defines a zonally symmetric temperature distribution in terms of a meridional and a vertical temperature gradient. Notably, if the Rossby number $Ro \equiv U/2\Omega L$ — with U denoting a characteristic zonal velocity, $L \sim a$ denoting a characteristic length scale (here taken as the planetary radius a), and Ω is the angular velocity of the planetary rotation — is kept constant, a reduction of the planetary radius a implies an increase in the rotation rate and, thus, a corresponding increase in the frictional/heating time factors that define the coefficients $k_{\mathbf{v}}, k_T$. Comparing the mean state of idealised climate simulations with planet radius $a = a_E$ and the NHD, NHS or HPE model formulation, respectively, we obtain indistinguishable results (not shown, cf. Wedi and Smolarkiewicz (2009)). Therefore, simulations are performed here for radius $a = a_E/20$ where $a_E = 6.371 \cdot 10^6$ m. The IFS is run with the currently operational set of 91 vertical levels and the top model level located at 0.01 hPa (model top at $p = 0$). In EULAG 40 vertical layers are used with a top-height fixed at 32 km. Both the IFS and EULAG start with identical initial conditions and use the same timestep $\Delta t = 15$ s. The equivalent gridlength of the simulations is 6.25 km. More details can be found in Wedi and Smolarkiewicz (2009). Figure 1 compares the zonal mean zonal flow of the NHD EULAG model simulation (panel a), the NHD IFS simulation (panel b), the QHE IFS simulation (panel c), the NHS IFS simulation (panel d), and the HPE IFS simulation[1] (panel e) averaged over the integration period of 275 simulation days (skipping the first 10 simulation days). A simulation day is defined as the time period of one planetary rotation. The NHD models and the QHE model develop a zonally-averaged easterly flow in the tropics between $200-600$ hPa which is absent in the NHS and in the HPE simulations and also absent in any of the model simulations (i.e. NHD,NHS,QHE or HPE) with $a = a_E$, cf. Wedi and Smolarkiewicz (2009). The occurrence of the easterly flow is in agreement with the easterly acceleration $\Delta U \lesssim -2\Omega H \cos\phi$ predicted from scale analysis in White and Bromley (1995), when the w-Coriolis term is considered in the zonal momentum equation. The effect is exaggerated with the increase in the rotation rate. Comparing the maximum easterly flow velocities at the equator in the NHD and QHE simulations on the reduced sphere, it is interesting to note that the QHE model simulation – like the scale analysis, cf. Wedi and Smolarkiewicz (2009) – shows a faster easterly jet core in the tropics compared to the NHD models for both EULAG and IFS as shown in Figs.1 (a)-(b), respectively. For NHS and HPE model there is simply no such easterly acceleration.

Investigating further if any influence on medium-range weather forecasts can be seen, the full ECMWF IFS model including the physical parametrizations (see Beljaars et al. (2004) for an overview) is used. Simulations are done for the period 2nd April 2007 00Z to 5th May 2007 00Z, every 24 hours with initial conditions from ERA-Interim (Dee and co authors, 2011). The horizontal resolution is T_L255 with 91 hybrid vertical levels. The forecast length of the 31 individual forecasts is 15 days. Anomaly correlation and root-mean-square (rms) error are calculated against the ECMWF operational analysis (suitably truncated) for the first 10 days of the forecast for geopotential height, winds and temperature using the HPE, QHE and NHD simulations, respectively. Again, we find indistinguishable results in the first 10 days (not shown). In order to assess if the differences are simply to small to be detected by standard scores, a finer measure has been applied. This has been shown to be useful in Jung and Vitart (2005), where the spatial standard deviation of the forecast difference for two sets of forecasts has been applied instead, to assess the importance of coupling an ocean model to the atmospheric model on the monthly time-scale. Later Wedi (2010) used this technique to illustrate the (non-)importance of the gravitational pull of the Moon on medium-range weather prediction. Figure 2 shows the spatial standard deviation of the forecast difference of the 500hPa geopotential height surface for several sets

[1] In this particular HPE IFS simulation the finite-element vertical discretisation was used.

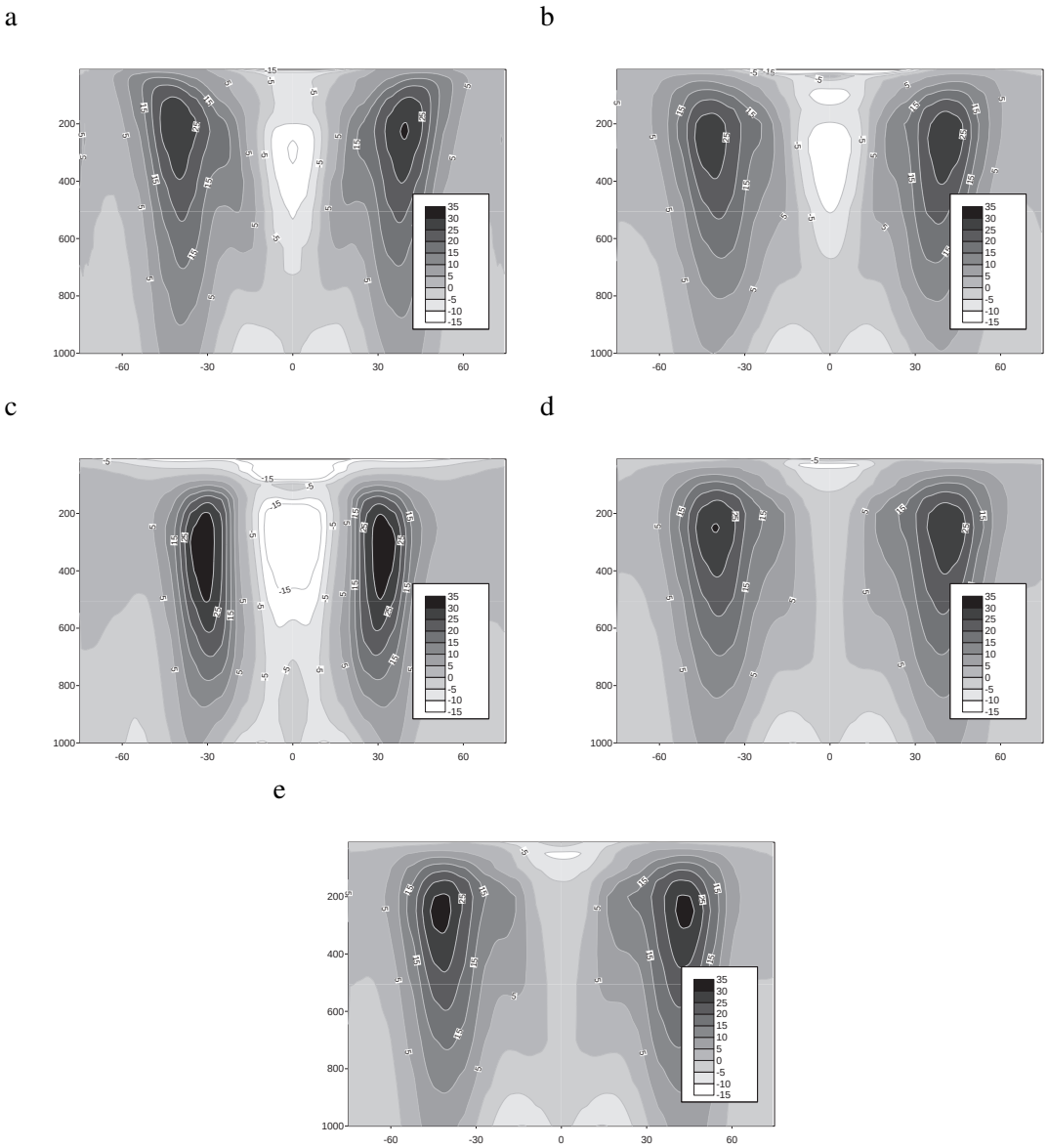

Figure 1: Held-Suarez dry climate simulations on the reduced-size sphere with depth ratio $r/a \approx 1/10$ ($a = a_E/20$) using (a) the EULAG NHD model, (b) the IFS NHD model, (c) the IFS QHE model, (d) the IFS NHS model, and (e) the IFS HPE model. The zonal mean zonal flow is averaged over 275 simulation days.

of 31 forecasts, NHD vs. HPE (deep NHD - shallow HPE) and QHE vs. HPE (deep QHE - shallow HPE). For reference, curves have been added for the spatial standard deviation of the forecast difference between two different model releases (35r2 - 32r3) and the difference between forecasts when every forecast of one ensemble was perturbed by a randomly-chosen single point perturbation of relative size 10^{-3} (random - control). The curves in figure 2 indicate that the difference is smaller than would be resulting from random single point perturbations and is significantly smaller than the difference between two model releases (in which the dynamical core was kept unchanged).

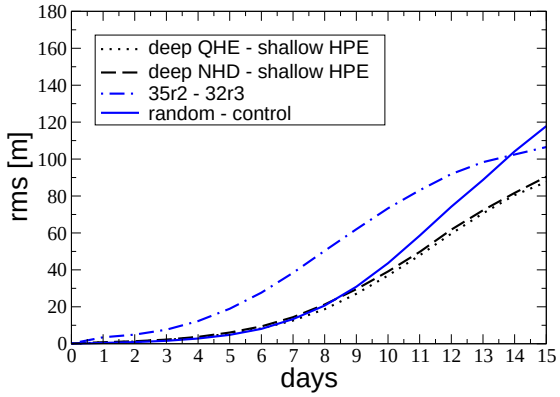

Figure 2: Spatial standard deviation (std) of the forecast difference of the 500hPa geopotential height surface between two sets of 31 forecasts,NHD vs. HPE (deep NHD - shallow HPE) and QHE vs. HPE (deep QHE - shallow HPE), respectively. As a reference the std of the forecast difference with a set of forecasts using random single point perturbations vs. HPE forecasts (random - control), and the std of the forecast difference between two meteorologically distinct model releases (35r2-32r3) have been added.

Finally, the four models — NHD, NHS, QHE and HPE — have been run as 13-months long integrations with four ensemble members, starting respectively on the 1st August 2000 00Z, the 2nd August 2000 06Z, the 3rd August 2000 12Z and the 4th August 2000 18Z. The simulations used a T159 resolution with 91 hybrid vertical levels (top full level at 0.01hPa). Initial conditions as well as prescribed daily SST and sea-ice fields at the lower boundary were provided from ERA-Interim. All four models used the same time-step $\Delta t = 3600$ s. Figure 3 illustrates the mean differences of the 500 hPa geopotential height over the northern hemisphere, with all simulations producing similar error patterns. The QHE model is perhaps slightly more different than the HPE, NHS and the NHD model. A further simulation (not shown) with the NHD model and using g rather than g_0 gives an almost identical pattern as shown in Fig. 3 (a), suggesting a negligible impact due to the vertical variation of g in this case. Comparisons of sfc parameters also show very small differences, as illustrated by total precipitation compared with observations for both the NHD IFS (Fig. 4) and the HPE IFS (Fig. 5). Figure 6 and 7 show the difference between HPE and NHD IFS model for zonally-averaged values of zonal and meridional wind, respectively, which equally show only small differences. In our experience these differences are smaller than what is typically obtained by changing details of the discretisation.

Although we do not find a significant influence of the NHD model in the hydrostatic regime, a significant influence can be shown on a reduced-size planet, even if the rotation rate is not accelerated. The canonical case of a trapped, horizontally propagating gravity wave (Wurtele et al., 1987; Keller, 1994) has been simulated with shallow- and deep-atmosphere, respectively. The setup is as described in Wedi and Smolarkiewicz (2009) but with an increased mountain amplitude of 500m. The EULAG domain size is $512 \times 228 \times 121$ with a horizontal and vertical grid spacing of 250 m, which corresponds to a

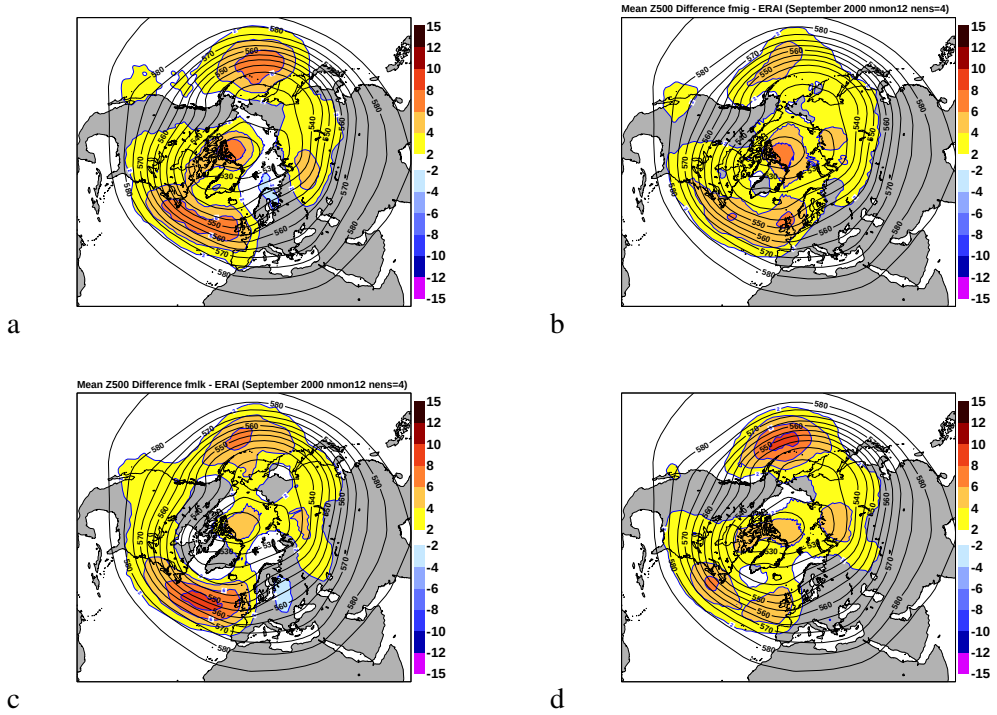

Figure 3: Average 500hPa geopotential height error compared to ERA-Interim for (a) the NHD IFS model, (b) the NHS IFS model, (c) the QHE IFS model, and (d) the HPE IFS model. The spatial error distribution is similar for all the simulations.

radius of the sphere $a = 20.3718$ km. The IFS is run with a T_L255 resolution with an equivalent linear reduced Gaussian grid (512 points along the equator) with 115 vertical levels. The lowest 15 km have the same vertical spacing of 250 m as in EULAG. Figures 8 (a)-(b) show the NHS simulations of IFS and EULAG, respectively. Figure 8 c) shows the NHD EULAG simulation. In the NHD simulation on the small planet the stratospheric gravity waves have a smaller amplitude, a shorter horizontal wavelength and the horizontal propagation of the waves is markedly slower, limiting the impact of the mountain in the lee in comparison to the NHS simulations. The QHE and HPE simulations both exhibit a lack of trapping in the vertical shear flow with an entirely vertical propagation of the gravity waves (not shown, see Wedi and Smolarkiewicz (2009)). The NHD IFS simulation is unstable for this case due to the large amplification factor arising from the ratio r/a on the small planet (see Table 1 in the appendix C).

4 Discussion and conclusions

The NHD formulation of Wood and Staniforth (2003) reduces the number of explicit metric terms — mainly in the continuity equation — by defining a new coordinate $\tilde{\Pi}$. When the depth of the atmosphere remains small compared to the radius of the planet, $\tilde{\Pi}$ remains close to Π. But the use of $\tilde{\Pi}$ in the dynamical core may still conflict with other parts of the model setup, such as during the initialisation of the model, the coupling to the physics (which remains unchanged, assuming a shallow atmosphere, in our tests), and the post-processing that is typically done on Π levels. Thus complex transformations between Π based quantities and $\tilde{\Pi}$ based quantities are required. This is not always easy to do exactly. Moreover, in the w equation the discretisation of the $\tilde{\Pi}$ form of the equation is more complicated than

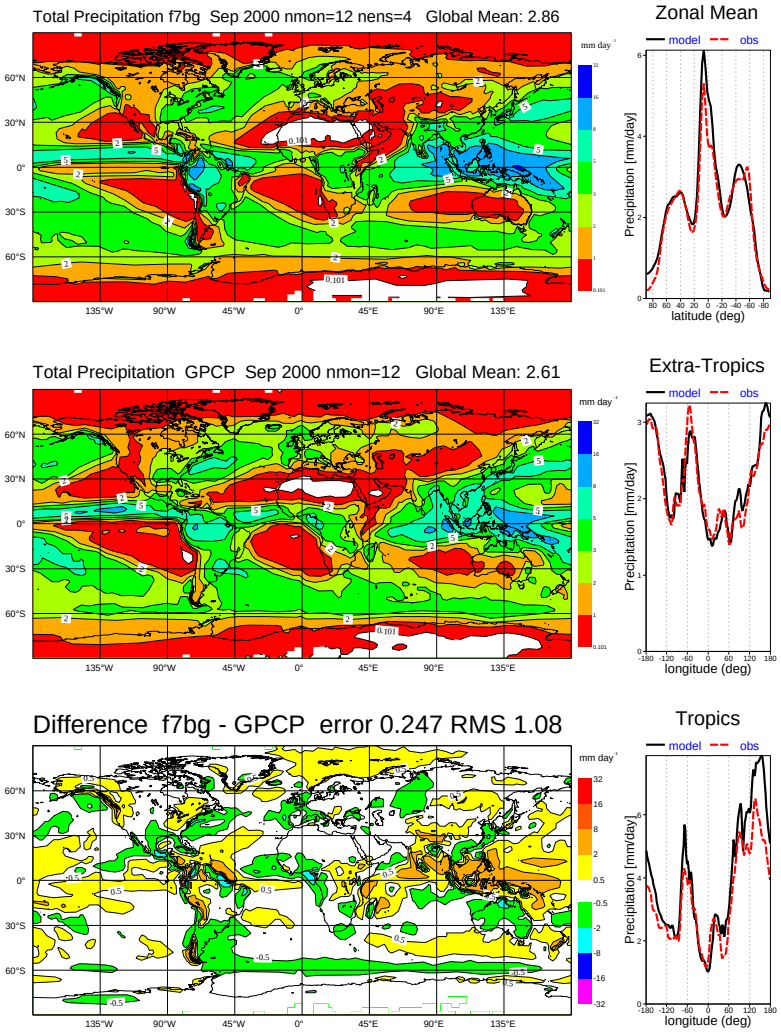

Figure 4: Ensemble average total precipitation compared to the Global Precipitation Climatology Project (GPCP) for the NHD IFS model.

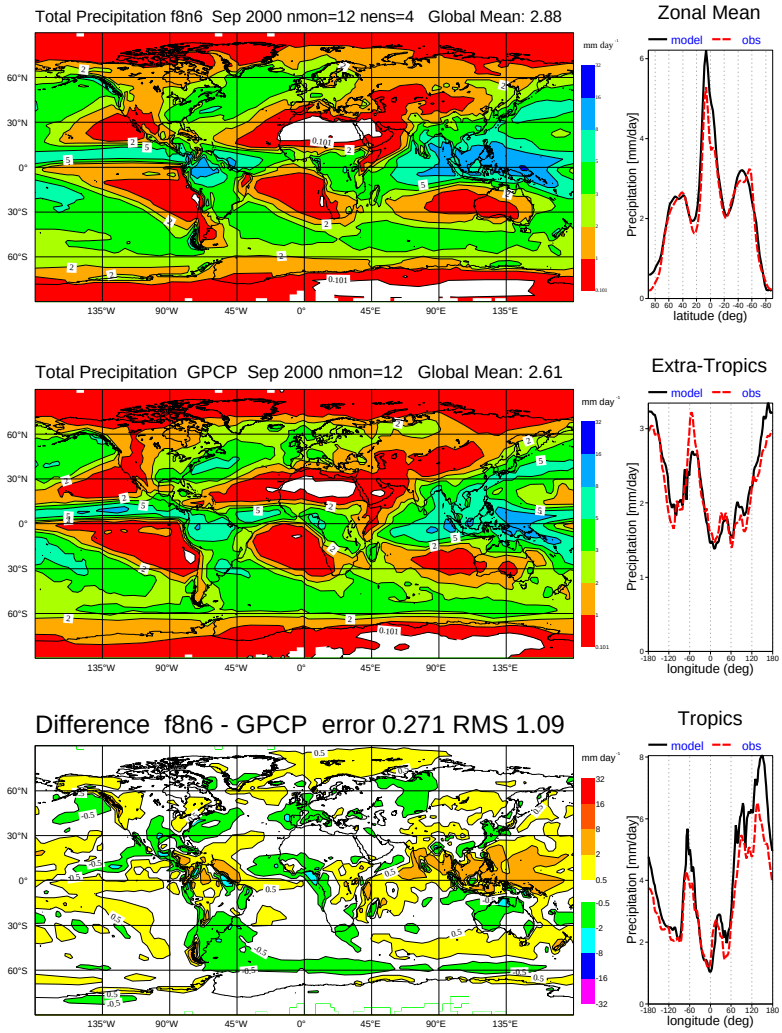

Figure 5: Ensemble average total precipitation compared to the Global Precipitation Climatology Project (GPCP) for the HPE IFS model.

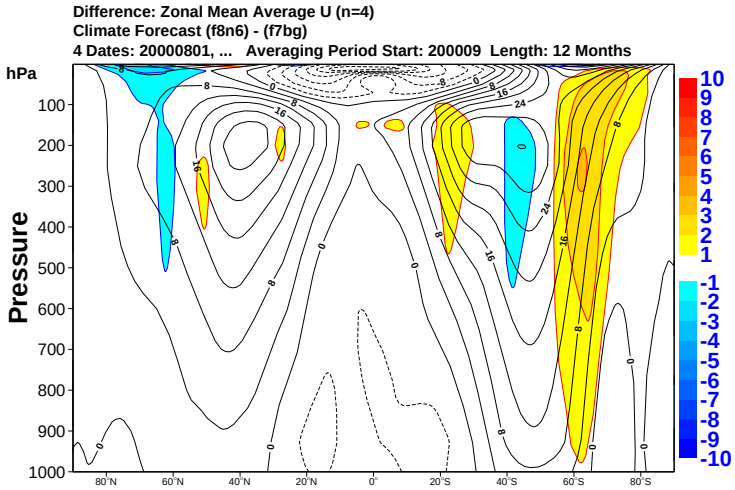

Figure 6: Ensemble average difference between the HPE minus NHD IFS model for zonally averaged zonal wind.

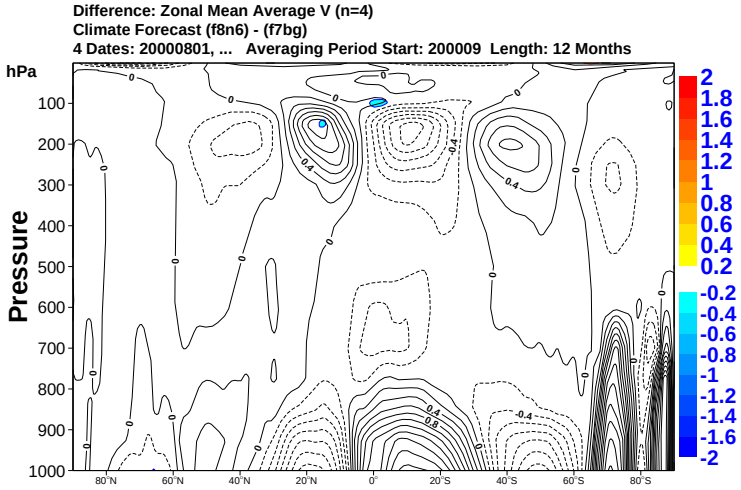

Figure 7: Ensemble average difference between the HPE minus NHD IFS model for zonally averaged meridional wind.

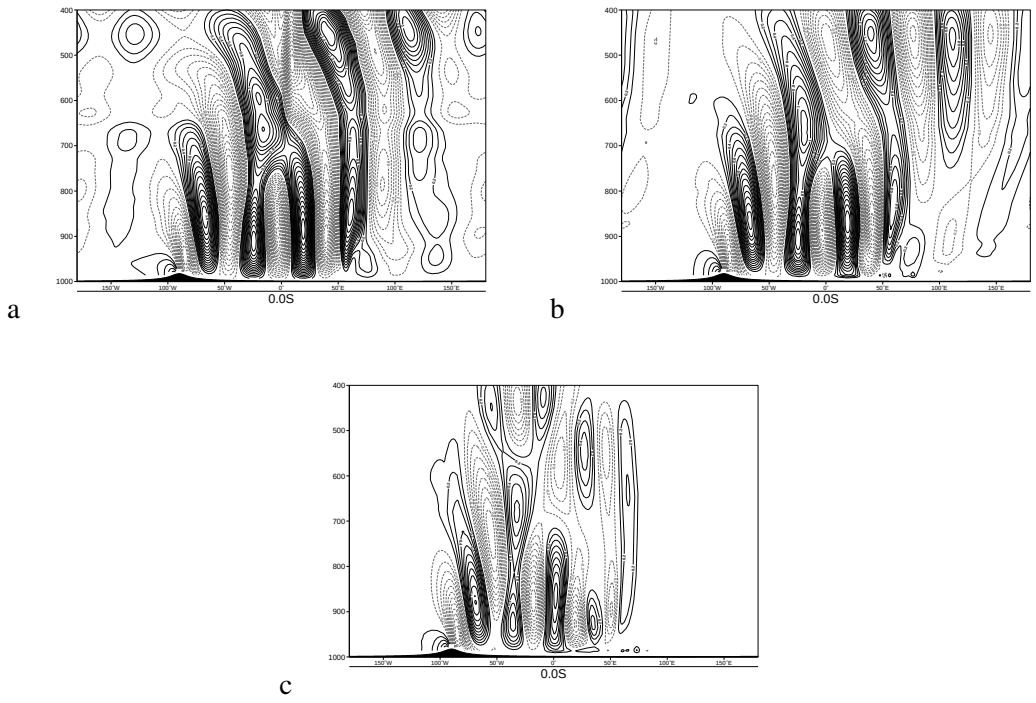

Figure 8: Vertical cross-section at the equator of vertical velocity after 75 minutes of simulation, comparing the NHS IFS model (panel a), the NHS EULAG model (panel b), and the NHD EULAG simulation (panel c) for a linearly-sheared flow past a quasi-two-dimensional "witch of Agnesi" obstacle on the sphere. The wind velocity is constant above 10.5 *km (or* $\approx$ 687 *hPa). Contour interval is* 0.1 ms^{-1}*. Solid/Dashed lines denote positive/negative contours. The vertical axis is pressure in hPa.*

for the equation formulated with Π. Instead of (36) the w equation may be solved directly as

$$\frac{dw}{dt} = -G\mu_s + g\frac{\partial(p-\Pi)}{\partial\Pi} + P_w, \tag{40}$$

but requiring additional transformations of Π based quantities and $\tilde{\Pi}$ based quantities to obtain the right-hand-side term. This would substantially complicate the existing code but may be explored in future. In the NHD formulation, terms such as $p-\tilde{\Pi}$ or $p/\tilde{\Pi}$ appear in the equations. For idealised reduced-size planet simulations, such quantities do not behave like $p-\Pi$ or p/Π and a change of the prognostic variable $\hat{Q}$ is required in combination with a second set of As and Bs (cf. appendix C) to obtain stable and accurate simulations in this case. However, if the aspect ratio of the vertical extent of the atmosphere compared to the radius of the sphere is not $\ll 1$ (cf. table 1), and despite the recalculation procedure of internal As and Bs, the usefulness of the present NHD formulation is limited. This has been found for linearly-sheared flow past a quasi-two-dimensional obstacle on the reduced-size sphere with radius $a = 20.3718$ km, when the present NHD formulation is unstable. Nevertheless, if considering potential future IFS applications with simulated atmospheric depths up to $\approx 600km$, i.e. $r^4/a^4 \approx 1.4$, this is not overly severe and the revised procedure appears to be stable for such aspect ratios.

When the resolved scales of the model simulations are hydrostatic, we have found that the nonhydrostatic deep-atmosphere (NHD), the nonhydrostatic shallow-atmosphere (NHS), the hydrostatic shallow-atmosphere (HPE), and the quasi-hydrostatic (QHE) model formulations give essentially the same results for both idealised climate (Held-Suarez) and for actual weather and climate simulations. However, we cannot exclude the possibility that a systematic signal may be extracted in longer integrations than the ones shown here. The results from the QHE model differed slightly more than one would have expected a-priori, both for the Held-Suarez simulation with accelerated rotation on the reduced-size planet, as well as in the 13 months integrations with physical parametrizations included. These differences cannot be attributed to the vertical variation of g. If these differences are not due to a coding error, they may be the result of introducing the pseudo-radius. However, in order to independently verify this, additional modifications are required to convert the NHD model to a quasi-hydrostatic version, which is beyond the scope of this paper. Moreover, the importance of the additional terms in the NHD model should be re-assessed, for example when weakly stratified boundary layers and sufficiently large vertical velocities are resolved rather than parametrized in global simulations on the sphere.

Acknowledgements: We would like to acknowledge the many colleagues and partners involved in the implementation of the non-hydrostatic limited-area version of ALADIN. Karim Yessad would also like to thank ECMWF and Meteo-France for the opportunity to stay at ECMWF in order to complete the adaptation of the NHS/NHD model in IFS. We are grateful to Nigel Wood for his thorough review of an earlier version of the manuscript. We are also grateful to Sylvie Lamy-Thepaut for improving the figures. Finally, comments from Agathe Untch and Pierre Bénard helped to improve the presentation.

A Derivation of the equations (23) (NHS model) and (38) (NHD model)

Starting with relation (37), the total derivative of d may be written as

$$\frac{dd}{dt} = \frac{d}{p}\frac{dp}{dt} - \frac{d}{T}\frac{dT}{dt} - \frac{d}{\tilde{m}}\frac{d\tilde{m}}{dt} - G\frac{p}{\tilde{m}R_dT}\frac{d}{dt}\left[\frac{\partial(r^2/a^2)w}{\partial\eta}\right]. \tag{41}$$

Using

$$\frac{d}{dt}\left(\frac{\partial(r^2/a^2)w}{\partial\eta}\right) = \frac{\partial}{\partial t}\left(\frac{\partial(r^2/a^2)w}{\partial\eta}\right) + \mathbf{V}\cdot\nabla\left(\frac{\partial(r^2/a^2)w}{\partial\eta}\right) + \dot{\eta}\frac{\partial}{\partial\eta}\left(\frac{\partial(r^2/a^2)w}{\partial\eta}\right) \tag{42}$$

and formulating the rhs in terms of $\partial/\partial\eta(...)$ gives

$$\frac{d}{dt}\left(\frac{\partial(r^2/a^2)w}{\partial\eta}\right)=\frac{\partial}{\partial\eta}\left(\left(\frac{\partial(r^2/a^2)w}{\partial t}\right)+\mathbf{V}\cdot\nabla\left[\frac{r^2}{a^2}w\right]+\dot{\eta}\frac{\partial(r^2/a^2)w}{\partial\eta}\right) \\ -\nabla\left[\frac{r^2}{a^2}w\right]\cdot\frac{\partial\mathbf{V}}{\partial\eta}-\frac{\partial(r^2/a^2)w}{\partial\eta}\frac{\partial\dot{\eta}}{\partial\eta}. \tag{43}$$

In above equation we have used

$$\begin{aligned}\mathbf{V}\cdot\nabla\left(\frac{\partial(r^2/a^2)w}{\partial\eta}\right)&=\frac{\partial}{\partial\eta}\left(\left[\frac{a}{r}\mathbf{V}\right]\cdot\left[\frac{r}{a}\nabla\right]\left(\frac{r^2}{a^2}w\right)\right)\\&-\frac{r}{a}\nabla\left[\frac{r^2}{a^2}w\right]\cdot\frac{\partial}{\partial\eta}\left[\frac{a}{r}\mathbf{V}\right]-\left[\frac{a}{r}\mathbf{V}\right]\cdot\nabla\left[\frac{r^2}{a^2}w\right]\frac{\partial}{\partial\eta}\left(\frac{r}{a}\right)\\&=\frac{\partial}{\partial\eta}\left(\left[\frac{a}{r}\mathbf{V}\right]\cdot\left[\frac{r}{a}\nabla\right]\left(\frac{r^2}{a^2}w\right)\right)-\nabla\left[\frac{r^2}{a^2}w\right]\cdot\frac{\partial\mathbf{V}}{\partial\eta}\\&+\left[\frac{a}{r}\mathbf{V}\right]\cdot\nabla\left[\frac{r^2}{a^2}w\right]\frac{\partial}{\partial\eta}\left(\frac{r}{a}\right)\\&-\left[\frac{a}{r}\mathbf{V}\right]\cdot\nabla\left[\frac{r^2}{a^2}w\right]\frac{\partial}{\partial\eta}\left(\frac{r}{a}\right)\end{aligned} \tag{44}$$

Using the continuity equation (cf. equation 4.9 in Wood and Staniforth (2003)) in the form

$$\frac{d\tilde{m}}{dt}+\tilde{m}\frac{r}{a}\nabla\cdot\left(\frac{a}{r}\mathbf{V}\right)+\tilde{m}\frac{\partial\dot{\eta}}{\partial\eta}=0 \tag{45}$$

noting the use of $(a/r)\mathbf{V}$ for the advection, re-grouping and multiplying by $-d/\tilde{m}$ gives

$$-\frac{d}{\tilde{m}}\frac{d\tilde{m}}{dt}=d\nabla\cdot\mathbf{V}+d\frac{\partial\dot{\eta}}{\partial\eta}-d\left(\frac{a}{r}\mathbf{V}\right)\cdot\nabla\left(\frac{r}{a}\right). \tag{46}$$

However, since the last term represents only a higher order correction, for ease of coding this term is dropped. Inserting (43), (46) and $D_3=(1/T)dT/dt-(1/p)dp/dt$ into equation (41) and noting the cancellation of the $\partial\dot{\eta}/\partial\eta$ terms, finally gives (cf. equation 38)

$$\frac{dd}{dt}=-dD_3+d\nabla\cdot\mathbf{V}-\frac{Gp}{\tilde{m}R_dT}\frac{\partial[d[(r^2/a^2)w]/dt]_{\mathrm{ad}}}{\partial\eta} \\ +\frac{Gp}{\tilde{m}R_dT}\left(\nabla\left[\frac{r^2}{a^2}w\right]\right)\cdot\frac{\partial\mathbf{V}}{\partial\eta}. \tag{47}$$

Equation (23) follows similarly but starting with $d\equiv-(g_0p/mR_dT)\partial w/\partial\eta$.

B Discretisation details of the NHD model

Most details of the (vertically) finite-difference discretisation are described in the literature (Ritchie et al., 1995; Bubnová et al., 1995; Bénard et al., 2010). Here we only highlight specific details due to the deep-layer formulation of the NHD model. Notably, IFS/Arpege is a spectral model and horizontal derivatives are calculated in spectral space. In order to minimise additional transforms when horizontal derivatives are required, typically these are expressed in terms of other more basic horizontal derivatives that are

already required elsewhere. In the vertical finite-difference model values are either kept on full-levels $_l$ or on in-between half-levels $_{\bar{l}}$.

Equation (30), to determine the radius r, is discretised on half levels as

$$r_{\bar{l}} = \left[r_{\rm s}^3 + \frac{3a^2}{G} \sum_{k=L}^{k=l+1} \frac{R_k T_k \tilde{\Pi}_k \tilde{\delta}_k}{p_k} \right]^{1/3}. \tag{48}$$

and on full-levels as

$$r_l = \left[r_{\bar{l}}^3 + \frac{3a^2}{G} \frac{R_l T_l \tilde{\Pi}_l \tilde{\alpha}_l}{p_l} \right]^{1/3}. \tag{49}$$

This discretisation on full levels is equivalent to writing $r_l^3 - r_{\bar{l}}^3 = (\tilde{\alpha}_l/\tilde{\delta}_l)(r_{\bar{l}-1}^3 - r_{\bar{l}}^3)$. An alternative discretisation for r_l would be

$$r_l - r_{\bar{l}} = (\tilde{\alpha}_l/\tilde{\delta}_l)(r_{\bar{l}-1} - r_{\bar{l}})$$

but this has not been tested.

The horizontal gradient of the radius is discretised on full levels as

$$\left[\frac{r}{a}\nabla\right] r_l = \frac{r_{\bar{l}}^2}{r_l^2} \left[\frac{r}{a}\nabla\right] r_{\bar{l}} + \frac{a^2}{G r_l^2} \left[\frac{r}{a}\nabla\right] \left[\frac{R_l T_l \tilde{\Pi}_l \tilde{\delta}_l}{p_l} \right] \tag{50}$$

and on half-levels as

$$\left[\frac{r}{a}\nabla\right] r_{\bar{l}} = \frac{r_{\rm s}^2}{r_{\bar{l}}^2} \left[\frac{r}{a}\nabla\right] r_{\rm s} + \frac{a^2}{G r_{\bar{l}}^2} \sum_{k=L}^{k=l+1} \left[\frac{r}{a}\nabla\right] \left[\frac{R_k T_k \tilde{\Pi}_k \tilde{\delta}_k}{p_k} \right] \tag{51}$$

with

$$\begin{aligned} \left[\frac{r}{a}\nabla\right] \frac{R_k T_k \tilde{\Pi}_k \tilde{\delta}_k}{p_k} =& \frac{T_k \tilde{\Pi}_k \tilde{\delta}_k}{p_k} \left[\frac{r}{a}\nabla\right] R_k \\ &+ \frac{R_k \tilde{\Pi}_k \tilde{\delta}_k}{p_k} \left[\frac{r}{a}\nabla\right] T_k \\ &+ \frac{R_k T_k \tilde{\delta}_k}{p_k} \left[\frac{r}{a}\nabla\right] \tilde{\Pi}_k \\ &+ \frac{R_k T_k \tilde{\Pi}_k}{p_k} \left[\frac{r}{a}\nabla\right] \tilde{\delta}_k \\ &- \frac{R_k T_k \tilde{\Pi}_k \tilde{\delta}_k}{p_k^2} \left[\frac{r}{a}\nabla\right] p_k \end{aligned} \tag{52}$$

noting that $\left[\frac{r}{a}\nabla\right] r_{\rm s} = \left[\frac{r}{a}\nabla\right] z_{\rm s}$.

The auxiliary quantities δ and α are useful in conversions when coupling to the physical parametrizations or for post-processing. In order to retrieve δ and α from $\tilde{\delta}$ and $\tilde{\alpha}$ when r is known, Π must be computed from $\tilde{\Pi}$ and r. Then the following approximation may be used for δ,

$$\delta \simeq \tilde{\delta} \frac{\tilde{\Pi}}{\Pi} \frac{a^2}{r^2} \frac{g}{G}, \tag{53}$$

and α is approximated by

$$\alpha \simeq \tilde{\alpha} \frac{\tilde{\Pi}}{\Pi} \frac{a^2}{r^2} \frac{g}{G}. \tag{54}$$

C Computing the vertical coefficients A,B internal to the NHD model

To accommodate idealised simulations on small planets, two sets of (A,B)s are defined, a pre-defined set denoted by $(A_{\rm F},B_{\rm F})$, which is identical for NHS and NHD simulations, and a set internal to the NHD model denoted by $(A_{\rm M},B_{\rm M})$. This appendix describes the conversion formulae, typical values and the iterative procedure applied to retrieve $\tilde{\Pi}$ and r when only Π is known from the initial conditions. Conversion formulae between $(A_{\rm F},B_{\rm F})$ and $(A_{\rm M},B_{\rm M})$ require the following steps:

- Define a reference surface pressure $\Pi_{\rm sr}$ (taken as 1013.25 hPa in NWP simulations).
- Compute $\Pi_{\rm r}$ from
$$\Pi_{\rm r} = A_{\rm F} + B_{\rm F}\Pi_{\rm sr}$$
- Diagnose r and $\tilde{\Pi}_{\rm r}$ at all model levels
- Compute $(A_{\rm M},B_{\rm M})$ from
$$A_{\rm M} = \frac{\tilde{\Pi}_{\rm r}}{\Pi_{\rm r}}A_{\rm F}$$
$$B_{\rm M} = \frac{\tilde{\Pi}_{\rm r}}{\Pi_{\rm r}}\frac{\Pi_{\rm sr}}{\tilde{\Pi}_{\rm s\ r}}B_{\rm F}$$

Note that $\tilde{\Pi} = A_{\rm M} + B_{\rm M}\tilde{\Pi}_{\rm s}$ is always valid; $\Pi = A_{\rm F} + B_{\rm F}\Pi_{\rm s}$ is valid only for one reference value of $\Pi_{\rm s}$ (i.e. $\Pi_{\rm sr}$). Table 1 compares the pre-defined values $(A_{\rm F},B_{\rm F})$ with the computed internal values $(A_{\rm M},B_{\rm M})$ for a reduced-size planet with radius $a = 100$ km using a typical tropospheric stratification with Brunt-Väisälä frequency $N = 0.01$ s^{-1}. For information the ratio r/a is added to illustrate the large range of values encountered leading to numerical instability in this case.

Table 1: A selection of ECMWF's operational set of 91 vertical levels $A_{\rm F}$, $B_{\rm F}$, Π and the corresponding set $A_{\rm M}$, $B_{\rm M}$, $\tilde{\Pi}$ for an idealised IFS simulation on a reduced-size planet with radius 100 km.

L	$A_{\rm F}$	$B_{\rm F}$	Π	$A_{\rm M}$	$B_{\rm M}$	$\tilde{\Pi}$	r/a
0	0	0.00000	0	0	0.00000	0	-
1	2	0.00000	2	33	0.00000	33	3.82
6	34	0.00000	34	380	0.00000	380	3.08
11	205	0.00000	205	1698	0.00000	1698	2.61
21	1714	0.00000	1714	9319	0.00000	9319	2.06
31	5663	0.00000	5663	23204	0.00000	23204	1.75
41	11983	0.00170	12153	40045	0.00342	40613	1.55
51	18717	0.04515	23232	51701	0.07503	64171	1.38
61	19785	0.22931	42717	44890	0.31301	96917	1.22
71	11543	0.58932	70475	21939	0.67384	133944	1.09
81	2356	0.89777	92133	4045	0.92726	158172	1.02
91	0	1.00000	100000	0	1.00000	166217	1.00

For the initial conditions one needs to retrieve $\tilde{\Pi}$ and r when only Π is known. An iterative algorithm is applied with the following steps:

- Save the original value of $\Pi_{\rm s}$.
- Save the original value of $p - \Pi$.
- Do a "first guess" iteration, with the following structure:

- compute a first guess for r (i.e. $r(iter=0)$), using formula (30) with Π instead of $\tilde{\Pi}$.
- compute $\tilde{\Pi}(iter=0)$ and $\tilde{\Pi}_s(iter=1)$ using formula (28).

- Do additional iterations:
  - start from $\tilde{\Pi}_s(iter)$, use the definition of the hybrid vertical coordinate to compute upper air $\tilde{\Pi}(iter)$.
  - use formula (30) with $\tilde{\Pi}(iter)$ to compute $r(iter)$.
  - use formula (28) to compute $\tilde{\Pi}_s(iter+1)$.

D Table of Symbols

Table 2: Description of symbols in the text.

Symbol	Description
Ω	Earth rotation angular velocity
θ	latitude
r	distance from the Earth centre
r_π	pseudo-radius
a	average Earth radius near the surface
g	gravity acceleration
G	constant reference value of g at $r=a$
g_0	constant gravity acceleration $g_0=G$
μ_s	Coriolis and advection term in the vertical component of the momentum equation
∇	horizontal gradient on η-surfaces
$A(\eta)$ and $B(\eta)$	functions defining the vertical hybrid coordinate
$\mathbf{k}=\mathbf{r}/r$	unit vertical vector
$\mathbf{r}$	vector directed radially outwards with length r
$\mathbf{V}$	horizontal wind
U and V	zonal and meridian components of horizontal wind
$\mathbf{V}_s$	surface horizontal wind
D	horizontal wind divergence
T	temperature
T_r	vertically varying reference temperature profile
q_i	tracer quantity
z	height
Φ	geopotential
$\Phi_s=gz_s$	surface geopotential (i.e. the orography)
$\omega=d\Pi/dt$	hydrostatic vertical velocity
$\tilde{\omega}=d\tilde{\Pi}/dt$	hydrostatic vertical velocity in the NHD model
w	true vertical velocity
$W=dr/dt$	pseudo-vertical velocity in the QHE model
d	vertical divergence
$\mathscr{X}$	difference between d_4 and d, cf. equation (20)
$d_4\equiv d+\mathscr{X}$	alternative vertical divergence

Continued on next page

Table 2 – continued from previous page

Symbol	Description
D_3	three-dimensional divergence
p	total pressure
p_s	total surface pressure
Π	hydrostatic pressure
$\Pi_s, \Pi_{S,r}$	hydrostatic surface pressure, and reference standard atmosphere equivalent, respectively
$\hat{Q}$	nonhydrostatic pressure departure variable
$\tilde{\Pi}$	mass-based vertically integrated quantity in the NHD model
$\tilde{\Pi}_s$	surface value of $\tilde{\Pi}$ in the NHD model
δ	depths of $\log\Pi$ (between two half levels)
$\tilde{\delta}$	depths of $\log\tilde{\Pi}$ (between two half levels) in the NHD model
α	depths of $\log\Pi$ (between a half level and a full level)
$\tilde{\alpha}$	depths of $\log\tilde{\Pi}$ (between a half level and a full level) in the NHD model
m	$\partial\Pi/\partial\eta$
$\tilde{m}$	$\partial\tilde{\Pi}/\partial\eta$ in the NHD model
R, R_d	gas constant for air and dry air, respectively
c_p	specific heat at constant pressure for air
c_v	specific heat at constant volume for air
$\mathbf{P_V}$	diabatic contribution to the horizontal components of the momentum equation
P_T	diabatic contribution to the thermodynamic equation
P_{q_i}	diabatic contribution to the tracer equation for tracer q_i
P_w	diabatic contribution to the w-form of the vertical component of the momentum equation
P_d	diabatic contribution to the d-form of the vertical component of the momentum equation

References

ALADIN (1997). The ALADIN project: Mesoscale modelling seen as a basic tool for weather forecasting and atmospheric research. *WMO Bull. 46*, 317–324.

Beljaars, A., P. Bechtold, M. Köhler, J.-J. Morcrette, A. Tompkins, P. Viterbo, and N. Wedi (2004). The numerics of physical parameterization. In *Proc. ECMWF Workshop on Recent Developments in numerical methods for atmosphere and ocean modelling*, Reading, UK, pp. 113–134. Eur. Cent. For Medium-Range Weather Forecasts.

Bénard, P. (2003). Stability of semi-implicit and iterative centered-implicit time discretizations for various equation systems used in NWP. *Mon. Weather Rev.*, 2479–2491.

Bénard, P. (2004). On the use of a wider class of linear systems for the design of constant-coefficients semi-implicit time schemes in NWP. *Mon. Weather Rev. 132*, 1319–1324.

Bénard, P., R. Laprise, J. Vivoda, and P. Smolíková (2004). Stability of leapfrog constant-coefficients semi-implicit schemes for the fully elastic system of Euler equations: Flat-terrain case. *Mon. Weather Rev. 132*, 1306–1318.

Bénard, P., J. Mašek, and P. Smolíková (2005). Stability of leapfrog constant-coefficients semi-implicit schemes for the fully elastic system of Euler equations: case with orography. *Mon. Weather Rev. 133*, 1065–1075.

Bénard, P., J. Vivoda, J. Mašek, P. Smolíková, K. Yessad, C. Smith, R. Brožková, and J.-F. Geleyn (2010). Dynamical kernel of the Aladin-NH spectral limited-area model: Revised formulation and sensitivity experiments. *Q.J.R. Meteorol. Soc. 136*, 155–169.

Bubnová, R., G. Hello, P. Bénard, and J.-F. Geleyn (1995). Integration of the fully elastic equations cast in the hydrostatic pressure terrain-following coordinate in the framework of the ARPEGE/Aladin NWP system. *Mon. Weather Rev. 123*, 515–535.

Dee, D. P. and . co authors (2011). The ERA-Interim reanalysis: configuration and performance of the data assimilation system. *Q.J.R. Meteorol. Soc. 137*, 553–597.

ECMWF (2000). In *Proc. 2000 Workshop on Developments in numerical methods for very high resolution global models*, Reading, UK. Eur. Cent. For Medium-Range Weather Forecasts.

Gerkema, T., J. T. F. Zimmerman, L. R. M. Maas, and H. van Haren (2008). Geophysical and astrophysical fluid dynamics beyond the traditional approximation. *Reviews Geophys. 46*(RG2004), 1–33.

Held, I. and M. Suarez (1994). A proposal for the intercomparison of the dynamical cores of atmospheric general circulation models. *Bull. Am. Meteorol. Soc. 73*, 1825–1830.

Jung, T. and F. Vitart (2005). Short-range and medium-range weather forecasting in the extratropics during wintertime with and without an interactive ocean. *Mon. Weather Rev. 134*, 1972–1986.

Keller, T. L. (1994). Implications of the hydrostatic assumption on atmospheric gravity waves. *J. Atmos. Sci. 51*, 1915–1929.

Laprise, R. (1992). The Euler equations of motion with hydrostatic pressure as an independent variable. *Mon. Weather Rev. 120*, 197–207.

Prusa, J. M., P. K. Smolarkiewicz, and A. A. Wyszogrodzki (2008). EULAG, a computational model for multiscale flows. *Comput. Fluids 37*, 1193–1207.

Ritchie, H., C. Temperton, A. Simmons, M. Hortal, T. Davies, D. Dent, and M. Hamrud (1995). Implementation of the semi-Lagrangian method in a high resolution version of the ECMWF forecast model. *Mon. Weather Rev. 123*, 489–514.

Robert, A. (1981). A stable numerical integration scheme for the primitive meterological equations. *Atmos. Ocean 19*, 35–46.

Robert, A., J. Henderson, and C. Turnbull (1972). An implicit time integration scheme for baroclinic models of the atmosphere. *Mon. Weather Rev. 100*, 329–335.

Simmons, A. J. and D. M. Burridge (1981). An energy and angular momentum conserving vertical finite difference scheme and hybrid vertical coordinates. *Mon. Weather Rev. 109*, 758–766.

Smolarkiewicz, P. K., V. Grubišić, L. G. Margolin, and A. A. Wyszogrodzki (1999). Forward-in-time differencing for fluids: Nonhydrostatic modelling of fluid motions on a sphere. Proc. 1998 Seminar on Recent Developments in Numerical Methods for Atmospheric Modelling, Reading, UK, pp. 21–43. Eur. Cent. For Medium-Range Weather Forecasts.

Staniforth, A., A. A. White, and N. Wood (2010). Treatment of vector equations in deep-atmosphere, semi-Lagrangian models. I: Momentum equation. *Q.J.R. Meteorol. Soc. 136*, 497–506.

Temperton, C. (1997). Treatment of the Coriolis terms in semi-Lagrangian spectral models. In *The Andre Robert Memorial Volume*, pp. 293–302. Canadian Meterological and Oceanographical Society.

Temperton, C., M. Hortal, and A. Simmons (2001). A two-time-level semi-Lagrangian global spectral model. *Q.J.R. Meteorol. Soc. 127*, 111–127.

Thuburn, J. and A. A. White (2012). A geometrical view of the shallow-atmosphere approximation, with application to the semi-Lagrangian departure point calculation. *Q.J.R. Meteorol. Soc.*. submitted.

Untch, A. and M. Hortal (2004). A finite-element scheme for the vertical discretization of the semi-Lagrangian version of the ECMWF forecast model. *Q.J.R. Meteorol. Soc. 130*, 1505–1530.

v. d. Toorn, R. and J. T. F. Zimmerman (2008). On the spherical approximation of the geopotential in geophysical fluid dynamics and the use of a spherical coordinate system. *Geophys. Astrophys. Fluid Dynamics 102*(4), 349–371.

Wedi, N. P. (2010). Diagnostics of model numerical cores: a model hierarchy. Proc. ECMWF Seminar on Diagnosis of Forecasting and Data Assimilation Systems, Reading, UK, pp. 191–203. Eur. Cent. For Medium-Range Weather Forecasts.

Wedi, N. P. and P. K. Smolarkiewicz (2009). A framework for testing global nonhydrostatic models. *Q.J.R. Meteorol. Soc. 135*, 469–484.

Wedi, N. P., K. Yessad, and A. Untch (2009). The nonhydrostatic global IFS/ARPEGE: model formulation and testing. Technical Report 594, Eur. Cent. For Medium-Range Weather Forecasts, Reading, UK.

White, A. A. and R. A. Bromley (1995). Dynamically consistent, quasi-hydrostatic equations for global models with a complete representation of the Coriolis force. *Q.J.R. Meteorol. Soc. 121*, 399–418.

White, A. A., B. J. Hoskins, I. Roulstone, and A. Staniforth (2005). Consistent approximate models of the global atmosphere: shallow, deep, hydrostatic, quasi-hydrostatic and non-hydrostatic. *Q.J.R. Meteorol. Soc. 131*, 2081–2107.

Wood, N. and A. Staniforth (2003). The deep-atmosphere Euler equations with a mass-based vertical coordinate. *Q.J.R. Meteorol. Soc. 129*, 1289 – 1300.

Wood, N., A. A. White, and A. Staniforth (2010). Treatment of vector equations in deep-atmosphere, semi-Lagrangian models. II: Kinematic equation. *Q.J.R. Meteorol. Soc. 136*, 507–516.

Wurtele, M. G., R. D. Sharman, and T. L. Keller (1987). Analysis and simulations of a troposphere - stratosphere gravity wave model. part I. *J. Atmos. Sci. 44*, 32693281.

Yessad, K. (2011). Dynamics. GmapDoc, http://www.cnrm.meteo.fr/gmapdoc/.